Since January 2020 Elsevier has created a COVID-19 resource centre with free information in English and Mandarin on the novel coronavirus COVID-19. The COVID-19 resource centre is hosted on Elsevier Connect, the company's public news and information website.

International Journal of Biological Macromolecules 207 (2022) 715–729

Contents lists available at ScienceDirect

International Journal of Biological Macromolecules

journal homepage: www.elsevier.com/locate/ijbiomac

Interfering effects on the bioactivities of several key proteins of COVID-19/variants in diabetes by compounds from Lianqiao leaves: *In silico* and *in vitro* analyses

Yishan Fu [a,1], Fei Pan [b,1], Lei Zhao [b], Shuai Zhao [a], Junjie Yi [a,*], Shengbao Cai [a,*]

[a] Faculty of Food Science and Engineering, Kunming University of Science and Technology, Kunming, Yunnan Province 650500, People's Republic of China
[b] Beijing Engineering and Technology Research Center of Food Additives, Beijing Technology and Business University, Beijing 100048, People's Republic of China

ARTICLE INFO

Keywords:
Angiotensin-converting enzyme 2
Diabetes
RBD domain

ABSTRACT

Diabetes is considered to be one of the diseases most associated with COVID-19. In this study, interfering effects and potential mechanisms of several compounds from Lianqiao (*Forsythia suspensa* (Thunb.) Vahl) leaves on the bioactivities of some key proteins of COVID-19 and its variants, as well as diabetic endothelial dysfunctions were illuminated through *in vitro* and *in silico* analyses. Results showed that, among the main ingredients in the leaves, forsythoside A showed the strongest docking affinities with the proteins SARS-CoV-2-RBD-hACE2 of COVID-19 and its variants (Alpha (B.1.1.7), Beta (B.1.351), and Delta (B.1.617)), as well as neuropilin-1 (NRP1), and SARS-CoV-2 main protease (M^{Pro}) to interfere coronavirus entering into the human body. Moreover, forsythoside A was the most stable in binding to receptors in Delta (B.1.617) system. It also has good antiviral activities and drug properties and has the strongest binding force to the RBD domain of COVID-19. In addition, forsythoside A reduced ROS production in AGEs-induced EA.hy926 cells, maintained endothelial integrity, and bound closely to protein profilin-1 (PFN1) receptor. This work may provide useful knowledge for further understanding the interfering effects and potential mechanisms of compounds, especially forsythoside A, from Lianqiao leaves on the bioactivities of key proteins of COVID-19/variants in diabetes.

1. Introduction

The COVID-19 outbreak began in December 2019 and was caused by the respiratory pathogen, severe acute respiratory syndrome coronavirus 2 (SARS-CoV-2) [1]. SARS-CoV-2 is a novel coronavirus, as SARS-CoV, belonging to the same large family of RNA viruses [2]. As well known, SARS-CoV-2 can cause respiratory, liver, neurological, and gastrointestinal diseases in humans, with the potential to cause severe and even fatal infections. The virus and its several variants have spread globally, with more than 200 million people infected worldwide as of August 2021 and the number is increasing, posing a huge threat to people's lives and health, as well as the globally economy [3]. The spike protein, also known as the S protein, is critical for the entering body of coronaviruses due to its binding ability to different host receptors [4]. In particular, the receptor binding domain (RBD) of spike protein fragment 1 (S1) of S protein binds to the angiotensin-converting enzyme 2 (ACE2) in the human body, which becomes a shortcut for the virus to invade the human body [5]. Up to now, SARS-CoV-2 has spawned a variety of mutants, and Alpha (B.1.1.7), Beta (B.1.351), and Delta (B.1.617) are the most widely spread mutants in the world, most of whose mutation points are in the RBD domain [6–8]. This suggests that mutations in this domain may be the main reason for the easy transmission and infection of the virus [9]. In addition, studies have shown that neuropilin-1 (NRP1), a protein present in human host cells, binds to the S protein, like ACE2, and acts as a helper to pull viruses into cells [10]. Previous studies have also identified a protease that plays a key role in mediating viral replication and transcription, namely SARS-CoV-2 main protease (M^{Pro}) [3]. Based on the important roles played by those protein receptors in this virus invasion, they have become potential targets for the design of drugs against the novel coronavirus. Therefore, interfering or hindering the bioactivities of those key proteins of SARS-CoV-2 and its variants may be an effective strategy to combat this outbreak.

It is found that diabetes is one of the diseases most associated with progression in patients infected with SARS-CoV-2; and diabetic patients

* Corresponding authors.
E-mail addresses: junjieyi@kust.edu.cn (J. Yi), caikmust2013@kmust.edu.cn, caikmust2013@163.com (S. Cai).
[1] These authors contributed equally to this work

https://doi.org/10.1016/j.ijbiomac.2022.03.145
Received 11 October 2021; Received in revised form 21 March 2022; Accepted 22 March 2022
Available online 26 March 2022

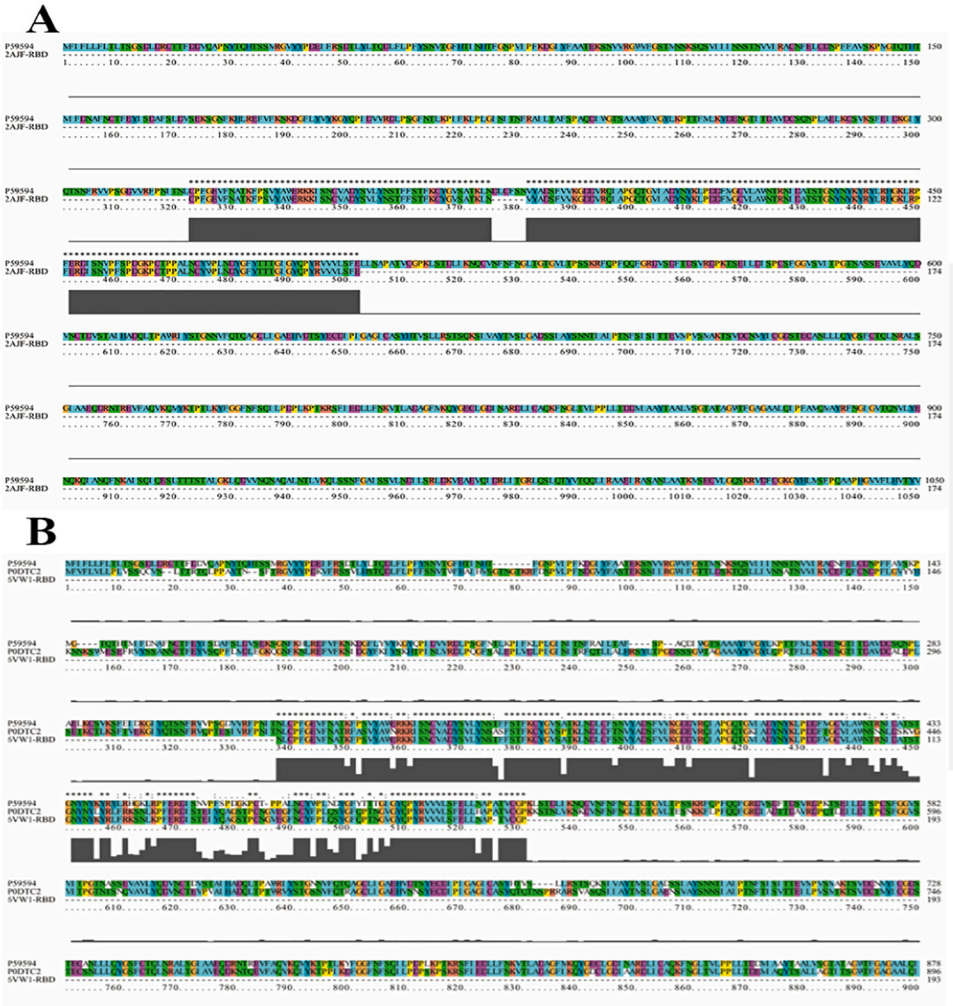

Fig. 1. The amino acid sequence alignment and pocket prediction. A, the amino acid residue sequence alignment of SARS-RBD-hACE2 protein (PDB ID: 2AJF) with a highly homologous amino acid sequence (P59594); B, the amino acid residue sequence alignment of SARA-CoV-2-hACE2 protein (PDB ID: 6VW1) with a highly homologous amino acid sequence P59594 and P0DTC2; C, the active pocket prediction after the complement of 2AJF and 6VW1.

are more susceptible to infection by SARS-CoV-2 and its variants, and are more likely to progress to severe condition and at higher risk of death, which is believed to be related to vascular endothelial dysfunction of diabetic patients to a certain extent [11,12]. It is well known that for diabetes, long-term hyperglycemia and oxidative stress can lead to the production and accumulation of advanced glycation end products (AGEs), which may induce endothelial cell damage through Profilin-1 (PFN1) protein, resulting in the recombination and redistribution of endothelial cytoskeleton actin to increase endothelial permeability and endothelial dysfunction [13]. ACE2, as a binding target for the virus to invade the human body, is widely found in vascular endothelial cells in the human body. When endothelial permeability and endothelial dysfunction increase, viruses become more easily invade the body through binding ACE2 in vascular endothelial cells to infect a person and cause severe complications [14–16]. Therefore, searching for a natural compound that can prevent AGEs-induced vascular endothelial dysfunction may be especially important for diabetic patients to deal with the infection of SARS-CoV-2 and its variants.

Lianqiao (*Forsythia suspensa* (Thunb.) Vahl), as a traditional herb, has many medicinal values. It is found that both the fruits and leaves of *F. suspensa* can regulate oxidative stress and pancreatic insulin secretion [17]. And the regulation of oxidative stress and/or pancreatic insulin secretion is considered to be important strategies for improving diabetes [18,19]. In addition, the fruits are more often used as a traditional Chinese medicine to treat plague or cold due to their antiviral effects [20]. The main bioactive ingredients in *F. suspensa* fruits are forsythoside A, forsythoside E, phillyrin, and chlorogenic acid [21,22], and forsythoside A has been proved to have the strongest antiviral effect [23]. Previous clinical and *in vitro* studies have shown that the traditional Chinese medicine formula Lianhua Qingwen exhibited good antiviral activity against SARS-CoV-2 [24,25], and *F. suspensa* fruits are one of the main herbs. Although *F. suspensa* fruits were not a food material, *F. suspensa* leaves, containing similar ingredients, have been authorized as a new food ingredient and commonly used as a kind of tea. However, there are currently no studies on the preventive mechanisms of infection of major components of *F. suspensa* leaves, especially forsythoside A, on the bioactivities of some key proteins of COVID-19 and its variants, or AGEs-induced endothelial dysfunction. Therefore, in this paper, *in silico*, and *in vitro* were used to compare and analyze the mechanisms of main components in *F. suspensa* leaves interfering the bioactivities of several key proteins of COVID-19 and its variants, and to further explore the protective effects on AGEs-induced endothelial dysfunction. Those results may provide new knowledge for further understanding the role of interfering the bioactivities of those key proteins of COVID-19/variants for diabetic patients to deal with the virus outbreak, and the potential interfering mechanisms of main compounds, especially forsythoside A, from Lianqiao leaves.

2. Materials and methods

2.1. Materials and reagents

Dulbecco's modified Eagle's medium (DMEM) and fetal bovine serum (FBS) were purchased from Gibco (Grand Island, NY, USA). Penicillin–streptomycin and 0.25% trypsin–EDTA solution were obtained from Solarbio (Beijing, China). Bovine serum albumin (BSA) was procured from Biorigin (Beijing, China). NO test kit (S0021S) was procured from Beyotime Biotechnology Co., Ltd. (Shanghai, China). SARS-CoV-2 Spike Protein (RBD, His Tag, Cat: 40592-V08H) and Human ACE2 (Fc Tag, Cat: 10108-H05H) protein was purchased from Sino Biological Co., LTD. (Beijing, China). Forsythoside A/forsythoside E/chlorogenic acid/hydroxychloroquine (purity: ≥95.0%) were purchased from Chengdu Must Biotechnology Co., Ltd. (Chengdu, Sichuan, China). Other chemicals and solvents were of analytical grade.

2.2. Model preparation and modeling

The proteins SARS-RBD-hACE2 (PDB ID: 2AJF) and SARS-CoV-2-RBD-hACE2 (PDB ID: 6VW1) were downloaded from the RCSB database (http://www.rcsb.org/pdb/home.do). The structure of all proteins was checked with Open-Source PyMOL (https://pymol.org), and SARS-CoV-2 in the 2AJF and 6VW1 structures were found. The loop area of the chimeric RBD area is missing the structure. Therefore, it is necessary to model their missing loop regions. First, the highly homologous amino acid sequences of 2AJF and 6VW1 (P59594) from the RCSB database was downloaded and the MEGA-X and Clustalx programs were used for comparison [26]. The results are shown in Fig. 1A and B. Among them, the sequence of the RBD region in P59594 and 2AJF is exactly the same. The missing amino acid residue sequence is 376-DLCFSN-381, and there are some differences between the RBD region sequence in the structure of P59594 and 6VW1. To determine the missing amino acid residue, in addition, a set of highly-homologous sequences (P0DTC2) was downloaded and compared, and the results showed that the missing amino acid residue in the structure was 522-A. The missing structure in the loop region of RBD was repaired by using the MODELLER 9.24 software package [27] for subsequent docking and kinetic studies. Mutations of Alpha (B.1.1.7), Beta (B.1.351), and Delta (B.1.617) were reported to focus on the RBD region, which was N501Y, N501Y, E484K and L452R, E484Q, respectively. Their structures were obtained by site-directed mutagenesis using the Swiss-pdbviewer software [28] using SARS-CoV-2 protein with chimeric RBD as the template.

2.3. Molecular docking analysis

AutoDock Vina [29] was used for molecular docking. There are eight kinds of proteins involved in docking, namely SARS-RBD-hACE2 (PDB ID: 2AJF) [30], SARS-CoV-2-RBD-hACE2 (PDB ID: 6VW1) [31], and Alpha (B.1.1.7), Beta (B.1.351) and Delta (B.1.617) completed in 2.3.1, and M^{Pro} (PDB ID: 6LU7) [3], NRPI (PDB ID: 6FMC) [32], PNF1 (PDB ID: 3NUL) [33] from the RCSB protein database. Small-molecule ligands of forsythoside A (CID: 5281773), forsythoside E (CID: 69634125), veklury (CID: 121304016), chlorogenic acid (CID: 1794427), phillyrin (CID: 101712), umifenovir (CID: 131411), and hydroxychloroquine (CID: 12947) were obtained from NCBI database (http://www.ncbi.nlm.nih.gov/pccompound). First, AutoDock Tools software (ADT, version 1.5.6) was used to add polar hydrogen atoms and Gastieger charges to the eight proteins and ligands. In order to obtain a reasonable docking position, according to previous studies, the functioning docking sites of 6LU7 and 6FMC were obtained [3,10], and the DoGSiteScorer tool was used for active pocket prediction for the remaining proteins (Fig. 1C) [34]. The docking process adopts semi-flexible docking, and the best docking result was judged by affinity. After the docking was completed, Open-Source PyMOL was used to observe the optimum conformation and hydrogen bond interaction, and Ligplot^{+} (Version v.2.2) was used to study the hydrophobic interaction [35]. The experiment was repeated three times, and the affinity value was expressed as mean ± SD.

2.4. Molecular dynamics analysis

The optimal conformation of molecular docking was used as the initial configuration, and the GROMACS 2019.5 package [36] was used to conduct a 100 ns molecular dynamics simulation for all systems to test the binding stability of the complexes. The topological parameters of forsythoside A were created using AmberTools and the AM1-BCC was given a fitting charge. TIP3P water molecules model was adopted for all systems. The Amber ff99SB-ILDN force field and the general Amber force field (GAFF) were used for classical molecular dynamics simulation [26]. The system was electrically neutral by adding counterions and 0.15 M NaCl. The steepest descent method was used for energy minimization of all systems (1000.0 kJ/mol/nm). After that, Canonical Ensemble (NVT, 1 ns) and Isobaric-isothermal Ensemble (NPT, 1 ns)

were performed to ensure that the system reached constant temperature and pressure (310.15 K, 1 Bar). Finally, the 100 ns MD simulation was started and the MD simulation was accelerated using the RTX 3090 GPU. Other parameters are referred to our previous study without specific instructions [37].

2.5. Analytical methods of computer simulation

The root-mean-square deviation (RMSD) of the selected element was calculated with the gmx *rms* program, which relative to its reference value is defined as:

$$\mathrm{RMSD} = \sqrt{\frac{1}{N}\sum_{i=1}^{N}(ri - r0)^2}$$

where r_i refers to the element position at time *i*; r_0 refers to the reference value [38]. The experiment was repeated 3 times, and RMSD after balancing was expressed as mean ± SD. The solvent accessible surface area (SASA) and radius of gyration (Rg) of the backbone atom were calculated with the *gmx gyrate* and *gmx sasa* program [36]. The trajectories were projected onto the RMSD and Rg from MD trajectories and according to the Boltzmann distribution to calculate the Gibbs free energy through Converting dot distribution to probability distribution (ddtpd) v1.3 program. According to these three columns date, the free energy landscape (FEL) was conducted [37,39].

2.6. Anti-SARS-CoV-2 activities and ADMET characteristics

Prediction of anti-SARS-CoV-2 activities of forsythoside A, forsythoside E, and chlorogenic acid was performed by using a machine learning platform (DrugCentral Redial). In addition, the drug-like properties of the three compounds, including absorption, distribution, metabolism, excretion, and toxicity (ADMET), were assessed by admetSAR, ADMET-pkCSM, and SwissADME [40–42].

2.7. Biolayer interferometry

The biolayer interference binding (BLI) experiment referred to the method in the report of Alexandra et al. [43]. The measuring instrument used was Octet non-labeled interaction instrument (SARTORIUS, Germany) with 1000 RPM oscillation at 30 °C. The Anti-His biosensor was soaked in PBS for 10 min and then incubated in 10× KB buffer for 1 min. The SARS-CoV-2 Spike Protein (RBD, His Tag) was formulated into a solution with a concentration of 50 μg/mL with 10× KB buffer. First, baseline equilibration was performed in the buffer for 120 s, and then the protein was loaded for 60 s, and equilibrated for 360 s. Human ACE2 (Fc Tag) protein/ forsythoside A/ forsythoside E/ chlorogenic acid/ hydroxychloroquine was diluted with 10× KB buffer to different concentrations and was bonded to the immobilized protein for 360 s, and then dissociated for 360 s. The 10× KB buffer was prepared in the following way: PBS (50 mL), BSA (50 mg), Tween (10 μL). The data were fitted with GraphPad Prism8 software. The baseline was subtracted from the data, and the combined part was selected for graphing.

2.8. Preparation of AGEs

AGEs were prepared through the reaction of fructose and BSA in accordance with the method reported by Zeng et al. [44]. with minor modifications. First, 1.5 g of BSA was dissolved in 50 mL of phosphate-buffered saline (PBS; pH 7.4, 0.2 M), and then the BSA solution (30 mg/mL) was incubated with or without 500 mM fructose for 60 days at 37 °C. After incubation, the reaction mixture was placed in a 10 kD dialysis bag and dialyzed in PBS (pH 7.4, 0.2 M) at 4 °C for 24 h. Thereafter, the AGEs were lyophilized and stored at −20 °C until use. Since the AGEs can exhibit self-fluorescence, the fluorescence value of the reaction products was measured for characterizing AGEs [45]. In the current study, the fluorescence value was measured at 370 nm excitation and 440 nm emission wavelengths by using a SpectraMax M5 microplate (Molecular Device, Sunnyvale, CA, USA). The AGEs-specific fluorescence value of the AGEs solution (equivalent to 1.0 mg/mL of BSA, 4582.07 ± 19.85) was significantly higher than that of the control group (1.0 mg/mL of BSA, 86.05 ± 4.81; $p < 0.05$), indicating that the AGEs were prepared well (Fig. S1).

2.9. ROS formation induced by AGEs in EA.hy926 cells

EA.hy926 cells were obtained from the Chinese Academy of Sciences Cell Bank (Kunming, China). The cells were cultured in a DMEM medium containing 10% fetal bovine serum (FBS) and 1% penicillin-streptomycin at 37 °C and 5% of CO_2. According to the method of Gisela et al., the method of AGEs-induced ROS production has been slightly modified [46]. Cells (1×10^5 cells/mL) were seeded into a six-well plate at 2.0 mL per well. After 24 h of incubation, according to the MTT results of each substance, each sample (forsythoside A, forsythoside E, chlorogenic acid, and hydroxychloroquine) was dissolved into a solution with a concentration of 20 μM in a medium containing AGEs (800 μg/mL). The control group was BSA (800 μg/mL), incubate for 24 h. Then, the cells were washed twice with PBS and incubated with 10 μmol/L dichlorodihydrofluorescein diacetate at 37 °C in the dark for 20 min. After incubation, the cells were washed twice with an FBS-free medium to prepare a cell suspension, and then the production of ROS was detected by a Guava easy Cyte 6-2 L flow cytometer (Millipore, Billerica).

2.10. AGEs-induced NO production in EA.hy926 cells

EA.hy926 cells (1×10^5 cells/mL) were seeded into a 96-well plate at 200 μL per well for 24 h and then incubated with 800 μg/mL of BSA or AGEs (with or without forsythoside A, forsythoside E, chlorogenic acid, and hydroxychloroquine) for another 24 h. The control group is 800 μg/mL BSA. After that, the cell supernatant was taken and measured according to the instructions of the detection kit. Cell viability in each corresponding well determined *via* MTT assays was used to normalize the cellular production of NO [46].

2.11. AGEs-induced changes in TEER value of EA.hy926 cells

The transepithelial electrical resistance (TEER) measurements can be used to check intercellular integrity and permeability. To detect the TEER value, the method reported by Wu et al. was used with some modifications [47]. EA.hy926 cells (1×10^5 cells/mL) were seeded into a chamber of Transwell 12-well plate at 500 μL per well. After 72 h of cultivation, BSA or AGEs medium (with or without forsythoside A, forsythoside E, chlorogenic acid, and hydroxychloroquine) was added. Resistance values were detected every 12 h by using a Millicell-ERS-2 voltmeter (Millipore Continental Water Systems, Bedford, MA, USA).

2.12. Statistical analysis

All experiments were performed at least twice, and experimental data was expressed as the mean ± SD. One-way ANOVA and Tukey's test were used to evaluate the significant differences ($p < 0.05$) using the Origin 8.5 software (OriginLab, Northampton, MA, USA).

3. Results and discussion

3.1. Molecular docking studies for prevention of COVID-19 and its variants

Studies have found that the RBD domain in the S1 subunit of SARS-CoV-2 is the host receptor interaction region, which is the most

Table 1
The binding abilities of small molecular compounds to 2AJF, 6VW1, 6 LU7, 6FMC, Alpha (B.1.1.7), Beta (B.1.351), and Delta (B.1.617).

Compounds	6FMC	6LU7	6VW1	2AJF	Alpha (B.1.1.7)	Beta (B.1.351)	Delta (B.1.617)
Forsythoside A	-7.8 ± 0.2^{b}	-9.0 ± 0.2^{c}	-10.2 ± 0.2^{f}	-9.3 ± 0.1^{e}	-10.2 ± 0.2^{e}	-10.3 ± 0.1^{f}	-10.2 ± 0.0^{f}
Forsythoside E	-7.7 ± 0.1^{b}	-8.0 ± 0.0^{b}	-8.7 ± 0.1^{e}	-8.6 ± 0.1^{d}	-8.8 ± 0.1^{d}	-8.8 ± 0.1^{e}	-8.7 ± 0.1^{e}
Veklury	-6.7 ± 0.2^{a}	-8.2 ± 0.1^{b}	-8.2 ± 0.1^{d}	-8.0 ± 0.1^{c}	-8.3 ± 0.0^{c}	-8.3 ± 0.1^{d}	-8.2 ± 0.1^{d}
Chlorogenic acid	-7.6 ± 0.2^{b}	-7.6 ± 0.2^{a}	-8.5 ± 0.1^{e}	-7.8 ± 0.2^{c}	-8.0 ± 0.1^{c}	-8.5 ± 0.0^{d}	-7.9 ± 0.0^{c}
Phillyrin	-6.9 ± 0.2^{a}	-7.5 ± 0.1^{a}	-7.8 ± 0.2^{c}	-8.0 ± 0.1^{c}	-8.0 ± 0.1^{c}	-8.0 ± 0.1^{c}	-7.8 ± 0.1^{c}
Umifenovir	–	–	-7.2 ± 0.1^{b}	-6.7 ± 0.1^{b}	-7.2 ± 0.0^{b}	-7.1 ± 0.1^{b}	-7.0 ± 0.1^{b}
Hydroxychloroquine	–	–	-6.1 ± 0.1^{a}	-6.2 ± 0.1^{a}	-6.0 ± 0.1^{a}	-6.0 ± 0.1^{a}	-6.2 ± 0.0^{a}

Affinity values (kcal/mol) are expressed as mean ± SD ($n = 3$). Different letters (a, b, c, d, e, f) in the same column indicated significant differences ($p < 0.05$).

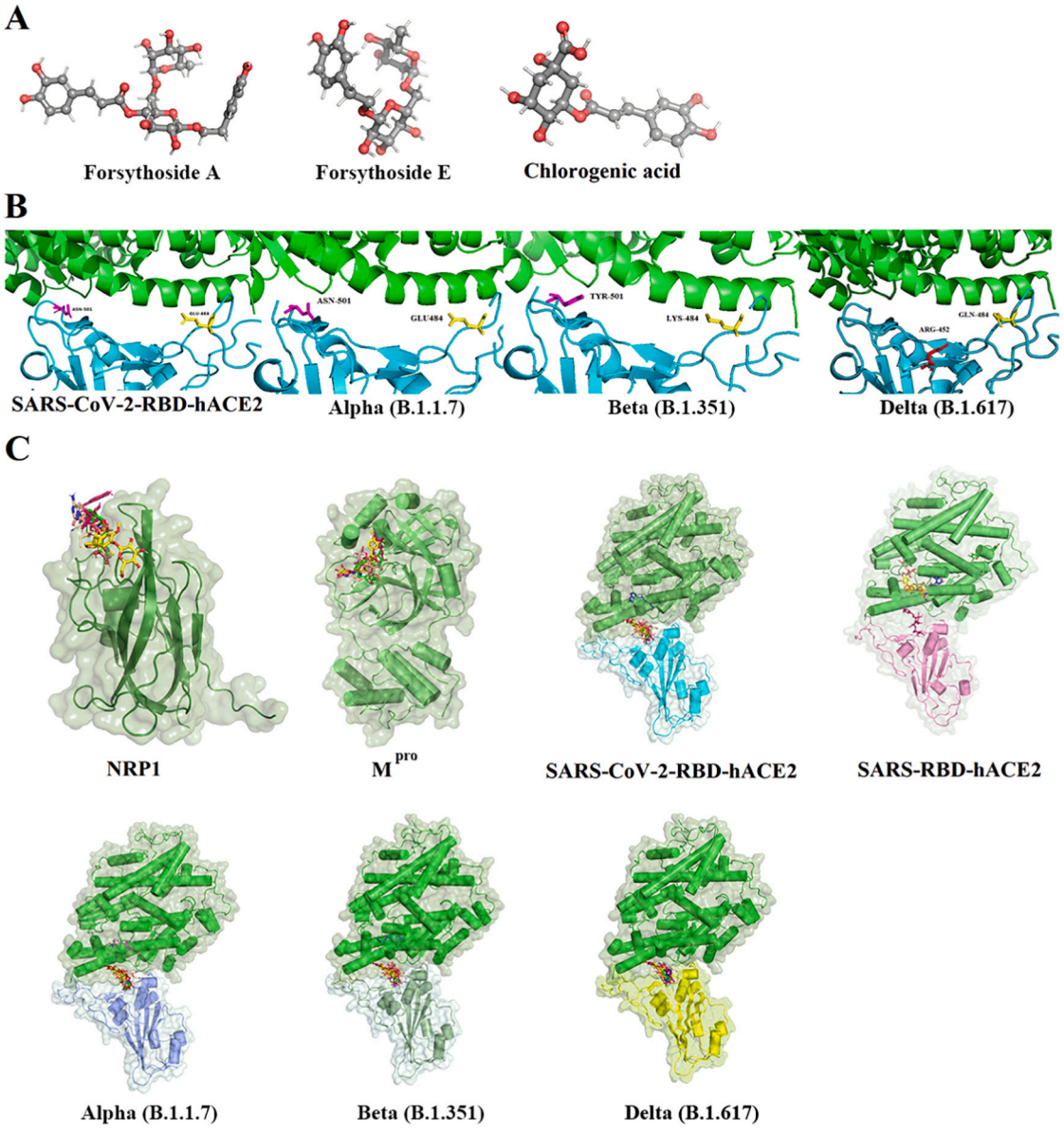

Fig. 2. The three-dimensional structure of forsythoside A/forsythoside E/chlorogenic acid in *F. suspensa* leaves (A), N501Y mutations, E484K, L452R, and E484Q mutations of RBD in 6VW1 (B), and the molecular docking results of several compounds with seven different proteins (C). In addition, in C, compounds are represented by distinctive colors. Forsythoside A is warmpink, forsythoside E is green, phillyrin is yellow, umifenovir is orange, veklury is wheat, chlorogenic acid is salmon, and hydroxychloroquine is blue. (For interpretation of the references to colour in this figure legend, the reader is referred to the web version of this article.)

important domain for the binding interaction between SARS-CoV-2 and ACE2 [31]. In addition, the rapid spread of SARS-CoV-2 may be related to a receptor called neuropilin-1 (NRP1), which binds to the CendR motif at the C-terminal of S1 protein to help the virus enter into the body [48]. The rapid spread may also be related to SARS-CoV-2 major protease (M^{pro}) that plays a key role in mediating viral replication and transcription [3]. In addition, SARS-CoV-2 is prone to mutations, and most of the mutation sites are in the RBD domain. The mutant virus not only propagates rapidly but is also more lethal [6–8].

In this study, SARS-RBD-hACE2 (PDB ID: 2AJF), SARS-CoV-2-RBD-

Table 2
Optimal results of molecular docking of forsythoside A with 2AJF, 6VW1, 6LU7, 6FMC and Alpha (B.1.1.7), Beta (B.1.351), and Delta (B.1.617).

Receptors for molecular docking	Affinity (kcal/mol)	Number of hydrophobic interactions	Amino acid residues involved in hydrophobic interactions	Number of hydrogen bonds	Amino acid residues involved in hydrogen bonds
6FMC	-7.8 ± 0.2^{a}	3	Tyr349, Thr316, Gly414	14	Ser346, Lys351, Tyr353, Asp320, Tyr297, Trp301, Asn300, Glu348
6 LU7	-9.0 ± 0.2^{b}	10	Glu166, Gln189, Asp187, His41, Tyr54, Thr45, Cys145, Asn142, Met165, His164	8	Leu-141, Glu166, Gly143, Thr24, Cys44, Arg188, Gln189, Gln192
6VW1	-10.2 ± 0.2^{c}	8	Leu29, Pro389, Asp405, Gly416, Tyr453, Ser494, Tyr495, Gln96	15	Gln96, Asn33, His34, Lys353, Gly496, Tyr505, Lys403, Gln409, Val417
2AJF	-9.3 ± 0.1^{b}	8	Thr402, Gly403, Val404, Asn479, Tyr481, Lys353, His34, Pro389	12	Tyr297, Tyr353, Lys351, Asp320, Ile415, Ser346, Trp301, Asn300
Alpha (B.1.1.7)	-10.2 ± 0.2^{c}	8	Pro389, Gln96, Asp405, Gly416, Tyr495, Tyr453, Ser494, Leu29	17	Gln96, Asn33, His34, Arg393, Glu37, Tyr495, Gly496, Lys353, Tyr505, Lys403, Gln409, Val417
Beta (B.1.351)	-10.3 ± 0.1^{c}	8	Pro389, Gln96, Asp405, Gly416, Tyr495, Tyr453, Ser494, Leu29	14	Gln96, Asn33, His34, Lys353, Gly496, Tyr505, Lys403, Gln409, Val417
Delta (B.1.617)	-10.2 ± 0.0^{c}	7	Leu29, Pro389, Asp405, Gly416, Tyr453, Ser494, Tyr495	11	Asn33, His34, Glu37, Gln96, Lys353, ARG393, Lys403, Gln409, Val417, Gly496, Tyr505

Affinity values are expressed as mean ± SD ($n = 3$). Different letters (a, b, c) indicated significant differences ($p < 0.05$).

hACE2 (PDB ID:6VW1), and mutated Alpha (B.1.1.7), Beta (B.1.351), Delta (B.1.617) were selected for molecular docking with active small molecules (forsythoside A, forsythoside E, chlorogenic acid, phillyrin), and veklury (inhibition of novel coronavirus activity), umifenovir (ACE2 inhibitor) and hydroxychloroquine (modified ACE2 receptor) were used as the positive control. In addition, the M^{Pro} (PDB ID: 6LU7) and the NRPI (PDB ID: 6FMC) were subjected to molecular docking with active small molecules (forsythoside A, forsythoside E, chlorogenic acid, phillyrin), and the positive control was veklury. The docking conformation and results were shown in Table 1 and Fig. 2C. The results showed that forsythoside A had the highest affinity (-7.8 ± 0.2 kcal/mol) for receptor 6FMC, while forsythoside E, chlorogenic acid, and phillyrin had higher affinity than veklury (-6.7 ± 0.2 kcal/mol). For receptor 6 LU7, forsythoside A had the highest affinity (-9.0 ± 0.2 kcal/mol, $p < 0.05$) compared with the other four compounds (veklury, forsythoside E, chlorogenic acid, and phillyrin). For receptor 6VW1, 2AJF, Alpha (B.1.1.7), Beta (B.1.351), and Delta (B.1.617), the affinity of forsythoside A was significantly higher than that of other compounds ($\leq -10.3 \pm 0.1$ kcal/mol, $p < 0.05$), followed by forsythoside E, while hydroxychloroquine was the lowest ($-6.0 \pm 0.1 \sim -6.2 \pm 0.1$ kcal/mol). Those results indicate that forsythoside A has the highest affinity to all seven proteins, even higher than the positive control, suggesting that forsythoside A may inhibit the invasion or transmission of SARS-CoV-2 and its mutants by widely binding multiple targets.

It is well known that the lumen of the protein can provide a strong hydrophobic environment and multiple hydrogen binding sites for the ligand, which contributes to the stability of the ligand [49]. In order to further understand the binding between forsythoside A and various receptors, the interactions between them were analyzed, including hydrogen bonds and hydrophobic interactions. As shown in Table 2 and Fig. 3, forsythoside A had the highest affinity with Beta (B.1.351) receptor, occurring hydrophobic interactions with 8 amino acids, and 14 hydrogen bonds with 9 amino acids. For 6VW1, Alpha (B.1.1.7), and Delta (B.1.617), forsythoside A formed 15, 17, and 11 hydrogen bonds with different amino acids, respectively, and hydrophobic interactions with 8 amino acids of all receptors. The affinities between forsythoside A and Beta (B.1.351), 6VW1, Alpha (B.1.1.7), and Delta (B.1.617) receptors were similar but significantly higher than those of other receptors ($p < 0.05$). The lowest affinity energy was found between forsythoside A and 6FMC, in which forsythoside A produced hydrophobic interactions with only 3 amino acids and 14 hydrogen bonds with 8 amino acids. For the receptor 6FMC, forsythoside A formed a hydrogen bond with Asp320, a key amino acid of 6FMC. Asp320 is an important binding site at the end of the CendR motif, which is connected by a salt bridge [48]. Therefore, forsythoside A may inhibit NRP1 binding to S protein by occupying the binding site at the end of the CendR motif. For receptor 6LU7, forsythoside A has hydrophobic interactions with Cys145, a key amino acid of 6LU7. A previous study has shown that some compounds that can covalently bind to Cys145 could effectively inhibit M^{Pro} activity and viral replication and transcription [50]. Therefore, forsythoside A may also inhibit the activity of M^{Pro} through hydrophobic interaction with Cys145, thus inhibiting the rapid propagation of the virus. In addition, forsythoside A formed hydrogen bonds with Lys353 of receptor 6VW1, Alpha (B.1.1.7), Beta (B.1.351), and Delta (B.1.617), respectively. Lys353, as a viral binding hotspot, connects with a salt bridge between Asp38 and Lys353, whose interaction could enhance the virus and the body's binding energy to facilitate the virus infection [51]. Thus, forsythoside A may disrupt salt bridges by binding to Lys353, thereby inhibiting viral activity.

3.2. Molecular dynamics studies on prevention of COVID-19 and its variants

Based on the molecular docking analysis in Section 3.1, forsythoside A was found to be associated with 7 receptors (NRP1, M^{Pro}, SARS-CoV-2-RBD-hACE2, SARS-RBD-hACE2, Alpha (B.1.1.7), Beta (B.1.351) and Delta (B.1.617)), and showed strong intermolecular interactions. Therefore, forsythoside A was selected for the next analysis by molecular dynamics simulation. The study simulated 100 ns MD for each system, using the GROMACS program to further elucidate the stability and more reliable binding patterns of forsythoside A with different protein complexes. The GROMACS program can reveal the interaction tracks between forsythoside A and different proteins, including root mean square deviation (RMSD), rotation radius (Rg), and solvent-accessible surface area (SASA). The calculated results were shown in Fig. 4.

RMSD and normal distribution are used to determine the mean deviation between the original time conformation and the complex at a specific time, and the combination of the normal distribution can evaluate whether the complex system reaches a stable state [52]. As shown in Fig. 4A and Fig. 4B, RMSD and the normal distribution of seven complexes were calculated. The results showed that the seven complexes all reached equilibrium within 100 ns, with RMSD values ranging from 0.05 to 0.45 (nm). The Delta (B.1.617) system had the best stability, and its distribution probability was the highest when its RMSD value was 0.225 ± 0.019 nm. Other protein systems, such as NRP1, SARS-CoV-2-RBD-hACE2, and SARS-RBD-hACE2, also showed a relatively stable state. Fig. 4C and D show the stability of forsythoside A in the complex system. The results show that forsythoside A is the most stable in the SARS-CoV-2-RBD-hACE2 system, with the minimum fluctuation within 100 ns. The distribution probability of RMSD at 0.275 ± 0.016 nm is the highest compared with other systems (Table S1). SASA and Rg can usually be used as characterization parameters to evaluate changes in

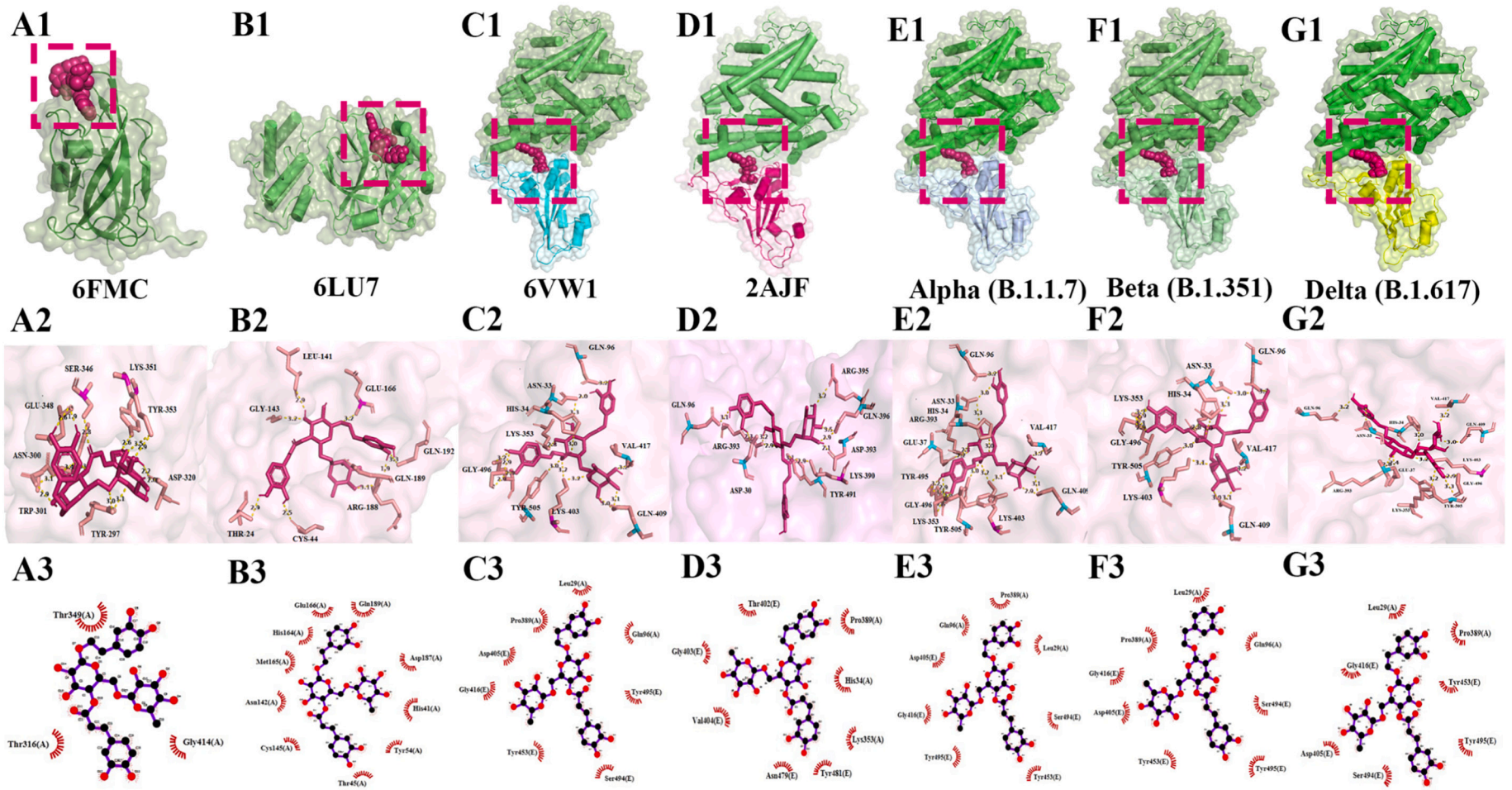

Fig. 3. Forsythoside A and A: NRP1 (6FMC), B: M^{pro} (6LU7), C: SARS-CoV-2-RBD-hACE2 (6VW1), D: SARS-RBD-hACE2 (2AJF), E: Alpha (B.1.1.7), F: Beta (B.1.351) and G: Delta (B.1.617) had the best conformation for molecular docking. The numbers 1–3 represent the binding site, hydrogen bond interaction, and hydrophobic interaction of forsythoside A and protein, respectively.

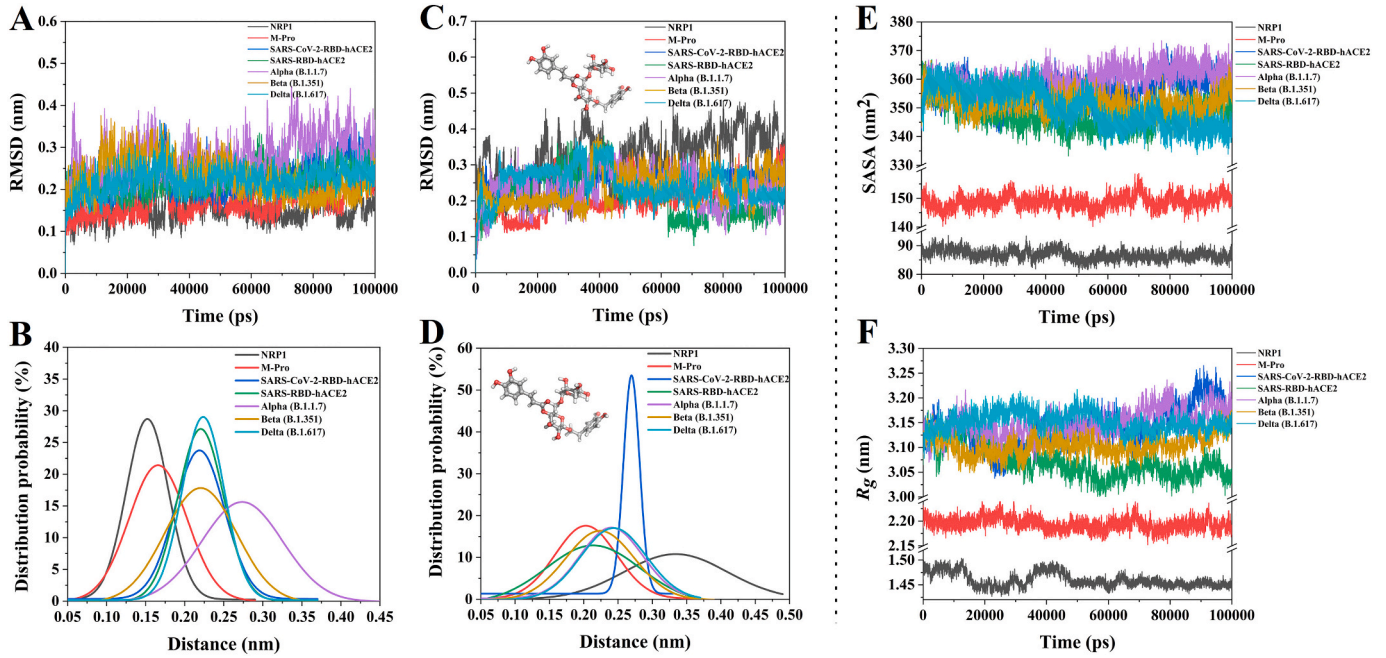

Fig. 4. Molecular dynamics results of forsythoside A complex with six receptors (NRP1, M^{Pro}, SARS-CoV-2-RBD-hACE2, SARS-RBD-hACE2, Alpha (B.1.1.7), Beta (B.1.351), Delta (B.1.617), and isolated ligand forsythoside A (100 ns). A1 and A2 are Root mean square deviations (RMSD, nm) of forsythoside A complex with seven receptors and the normal distribution results for all points in A1. B1 and B2 are RMSD of forsythoside A complex extracted separately and the normal distribution results for all points in B1. C is the Radius of gyration (Rg) and D is solvent accessible surface area (SASA) values.

protein structure [53], and the balance of the system can make the structure of the compound more compact. The changes of SASA and Rg in the protein backbone in the presence of forsythoside A were calculated by the *gmx sasa* and *gmx gyrate* program. As shown in Fig. 4E, the SASA values of NRP1, M^{Pro}, and Beta (B.1.351) did not change significantly during the whole simulation process, fluctuating at 85, 150, and 360 nm^2, respectively. It indicated that the binding region of forsythoside A had little effect on the structure of NRP1, M^{Pro}, and Beta (B.1.351). In addition, the SASA values of SARS-RBD-hACE2, and Delta (B.1.617) decreased from 360 nm^2 to 340 nm^2 and 360 nm^2 to 350 nm^2 respectively, especially in Delta (B.1.617) system, which remained stable after 80 ns. This indicates that the combination of forsythoside A makes the structure of SARS-RBD-hACE2 and Delta (B.1.617) more compact, especially Delta (B.1.617), whose structure is more stable. Similar results can also be obtained from Fig. 4F. Rg values of NRP1, M^{Pro} and Beta (B.1.351) did not change significantly during the whole simulation process, fluctuating at 1.45, 2.20 and 3.10 nm, respectively. The Rg values of SARS-RBD-hACE2 and Delta (B.1.617) decreased significantly at 60 ns, indicating that the structure of SARS-RBD-hACE2 and Delta (B.1.617) became more compact after MD simulation. Previous studies have also shown that ligand binding reduces the denseness of proteins and makes them more compact [52,54]. In addition, Fig. 5 is the energy landscape map obtained from RMSD and Rg, and the complex structure at 0 ns (initial state), the lowest free energy point (most stable state), and 100 ns (final state) are extracted from the molecular dynamics simulation. Fig. 5 can clearly reflect the position and protein structure changes of small molecule forsythoside A in the process of molecular dynamics at different times. For example, in Fig. 5G, combined with the results of molecular dynamics, it can be seen that when Delta (B.1.617) is in the most stable state, its protein structure is more compact, and the ligand moves within the active pocket range, indicating that the complex has high stability and good binding effect.

3.3. Anti-SARS-CoV-2 activities and ADMET characteristics of three active substances in Forsythia suspensa leaves by machine learning platform

Based on the results of molecular docking, a machine learning platform was used for further carrying out the next step of research on the three compounds (forsythoside A, forsythoside E, and chlorogenic acid) with high docking affinity with the receptor (SARS-CoV-2-RBD-hACE2, NRP1, M^{Pro}, Alpha (B.1.1.7), Beta (B.1.351) and Delta (B.1.617)). The anti-SARS-CoV-2 activity of forsythoside A, forsythoside E, and chlorogenic acid in *F. suspensa* leaves was predicted through the machine learning platform the REDIAL-2020 server [55]. As shown in Table 3, the program predicts 5 modules, namely Live Virus Infectivity, Viral Entry, Viral Replication, *in vitro* Infectivity and Host Protein. As shown in Table 3, those three compounds are inactive for the Live Virus Infectivity module, which means that they may not prevent the new coronavirus from infecting the human body by repairing the function of infected cells. The spike-ACE2 protein-protein interaction (AlphaLISA) of the viral entry module, which measures whether compounds can disrupt the interaction between viral S proteins and ACE2, found that forsythoside A is active, illustrating that forsythoside A may hinder viral entry by hindering the binding of S proteins to ACE2, while the other two compounds are inactive. For the Viral Replication module, it predicts whether the compound has the ability to disrupt virus replication. However, the results show that none of these three substances have this activity. For the *In vitro* Infectivity module, this module uses the fusion of coronavirus (SARS, MERS) and murine leukemia virus core to produce pseudotyped particles. Since they all have spiked proteins, they can be used to predict and imitate the entry of new coronaviruses. The pseudotyped particle assay measures the inhibition of virus entry in the cell. It is obvious from the table that forsythoside A, forsythoside E, and chlorogenic acid are all active for SARS-CoV pseudotyped particle entry (CoV-PPE) detection. This showed that all three compounds may act by inhibiting the entry of viruses in cells. The last module was Host Protein, and none of the three compounds had any activity, suggesting that SARS-CoV-2 invasion might not be prevented in this way.

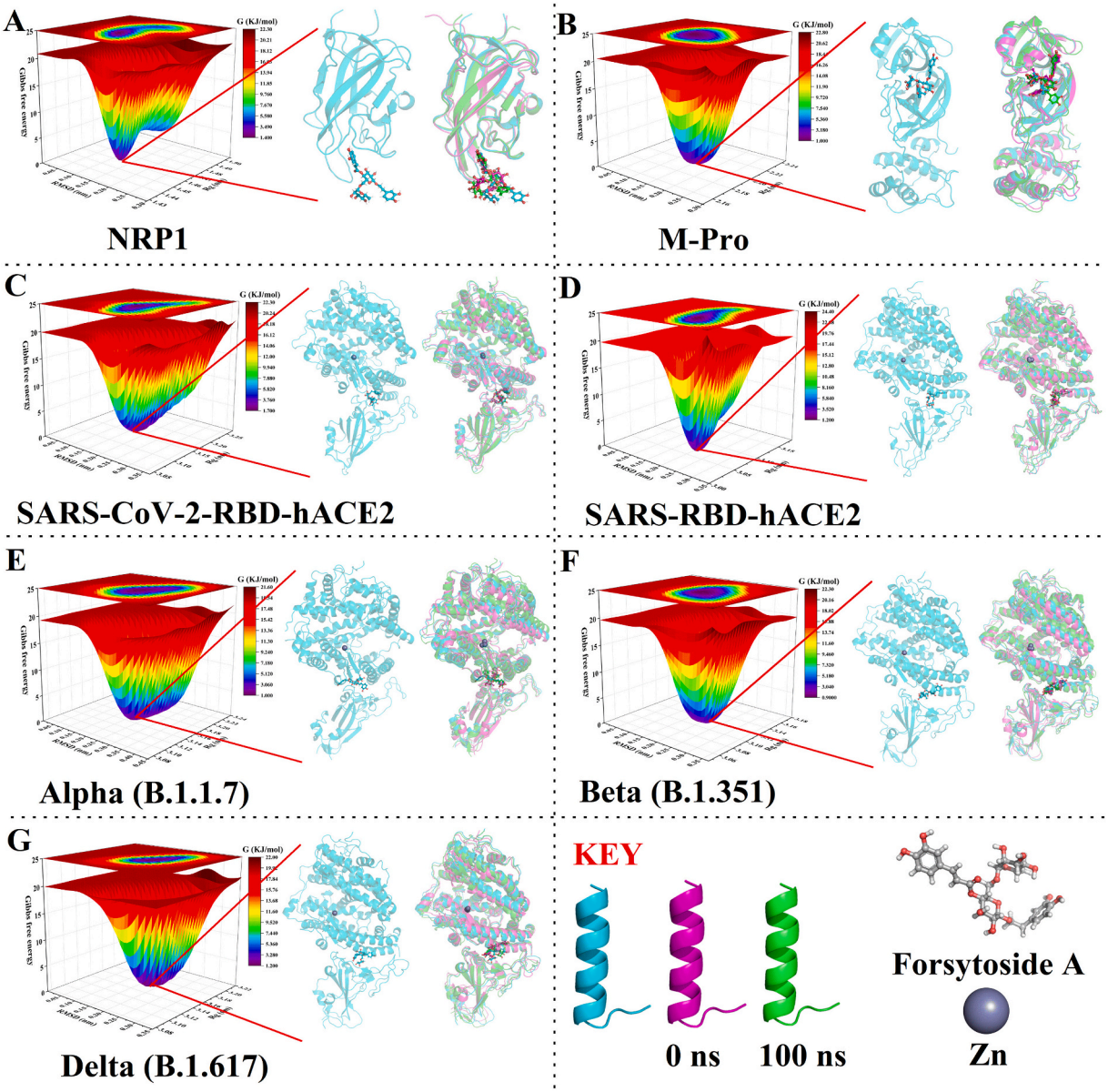

Fig. 5. The free energy landscapes and lowest energy conformation (cyan) comparison (0 ns, magenta; 100 ns, green). (For interpretation of the references to colour in this figure legend, the reader is referred to the web version of this article.)

Table 3
Prediction result of anti-SARS-CoV-2 activities of main functional components of *F. suspensa* leaves by machine learning in REDIAL-2020.

Performance	Class	Forsythoside A		Forsythoside E		Chlorogenic acid	
		Prediction	Confidence	Prediction	Confidence	Prediction	Confidence
Live Virus Infectivity	SARS-CoV-2 cytopathic effect (CPE)	Inactive	0.96	Inactive	0.91	Inactive	1
	SARS-CoV-2 cytopathic effect (host tox Counter) / Cytotoxicity	Inactive	0.8	Inactive	0.79	Inactive	1
Viral Entry	Spike-ACE2 protein-protein interaction (AlphaLISA)	Active	0.88	Inactive	0.86	Inactive	1
	Spike-ACE2 protein-protein interaction (TruHit Counter)	Active	0.77	Inactive	0.54	Inactive	1
	ACE2 enzymatic activity	Active	0.58	Inactive	0.74	Inactive	1
Viral Replication	3CL enzymatic activity	Inactive	0.69	Inactive	0.79	Inactive	1
In vitro Infectivity	SARS-CoV pseudotyped particle entry (CoV-PPE)	Active	0.62	Active	0.56	Active	0.5
	SARS-CoV pseudotyped particle entry counter screen (CoV-PPE_cs)	Inactive	0.44	Active	0.55	Inactive	0.77
	MERS-CoV pseudotyped particle entry (MERS-PPE)	Active	0.45	Inactive	0.8	Inactive	0.89
	MERS-CoV pseudotyped particle entry counter screen (MERS-PPE_cs)	Inactive	0.66	inactive	0.66	inactive	0.68
Host Protein	Sigma1 Receptor (sigma1R)	Inactive	0.97	inactive	0.96	inactive	0.96

Table 4
The ADMET properties of main functional components of *F. suspensa* leaves were predicted using three machine learning servers (admetSAR, ADMET-pkCSM and SwissADME).

Parameter	admetSAR			ADMET-pkCSM			SwissADME		
	Forsythoside A	Forsythoside E	Chlorogenic acid	Forsythoside A	Forsythoside E	Chlorogenic acid	Forsythoside A	Forsythoside E	Chlorogenic acid
Glycoprotein substrate	Yes	Yes	Yes	Yes	Yes	Yes	NO	Yes	NO
glycoprotein inhibitor	No	No	No	No	No	No	\	\	\
CYP450 2C9 Substrate	No	No	No	\	\		\	\	
CYP450 2D6 Substrate	No	No	No	No	No	No		\	\
CYP450 3A4 Substrate	No	No	No	No	No	No	\	\	\
CYP450 1A2 Inhibitor	No	No	No	No	No	No	No	No	No
CYP450 2C9 Inhibitor	No	No	No	No	No	No	No	No	No
CYP450 2D6 Inhibitor	No	No	No	No	No	No	No	No	No
CYP450 2C19 Inhibitor	No	No	No	No	No	No	No	No	No
CYP450 3A4 Inhibitor	No	No	No	No	No	No	No	No	No
AMES Toxicity	No	No	No	No	No	No	\		\
Hepatotoxicity	\	\	\	No	No	No	\	\	\
Carcinogenicity (Three-class)	No	No	No	\	\	\	\	\	\

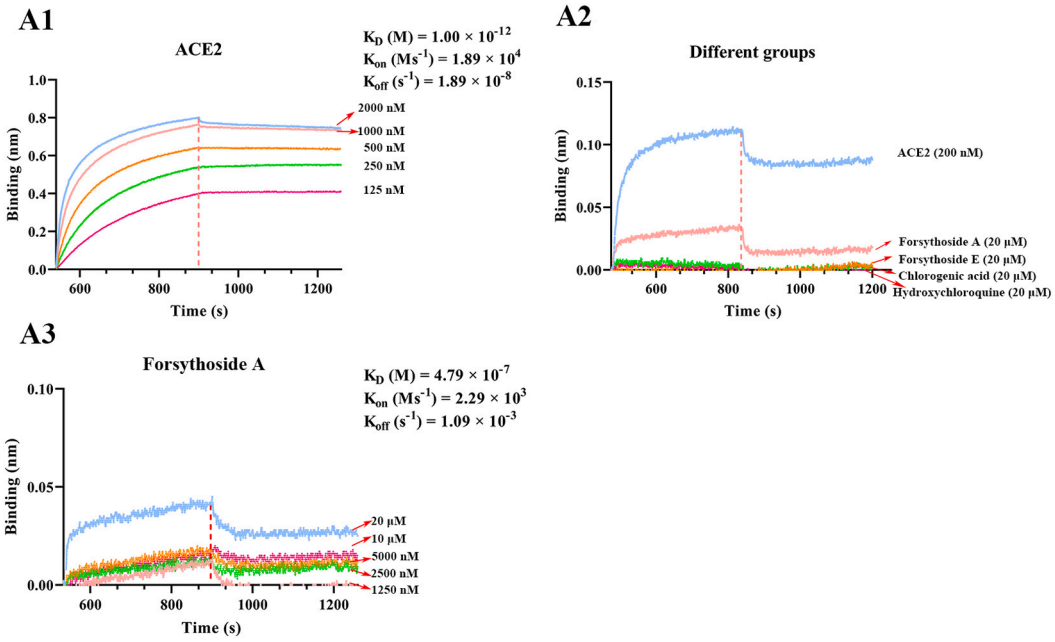

Fig. 6. The association and dissociation of SARS-CoV-2-RBD with different substances were detected by the OCTET system. A is the result of the association and dissociation of SARS-CoV-2-RBD with different concentrations of hACE2. B is the association and dissociation result of SARS-CoV-2-RBD and five substances (hACE2, forsythoside A, forsythoside E, chlorogenic acid, and hydroxychloroquine). C is the result of the association and dissociation of SARS-CoV-2-RBD and forsythoside A at different concentrations.

In addition, the properties of the compound itself should be considered when it enters the body. Three servers (admetSAR, ADMET-pkCSM, and SwissADME) were used to predict the ADMET characteristics of forsythoside A, forsythoside E, and chlorogenic acid [40–42]. ADMET represents several characteristics of absorption, distribution, metabolism, excretion, and toxicity, which helps to identify candidate molecules that can be clinically successful in the process of drug design [56]. The results are shown in Table 4. In the absorption process, P-glycoprotein is an important transporter. If the compound has an inhibitory effect on these transporters, it may interfere with the pharmacokinetics of other compounds. As shown in Table 4, those three compounds are not P-glycoprotein inhibitors, indicating that they will not affect the absorption of other substances. In the process of metabolism, drug-metabolizing enzymes are an important factor affecting pharmacokinetics. The cytochrome P450 (CYP) family is an important detoxification enzyme in the human body, which mainly exists in the liver, especially CYP450 3A4, which is the main metabolizing enzyme of drugs. When substances enter the human body to participate in metabolism, if the changes in the activity of these enzymes are affected, it may cause pharmacokinetic disorders. As shown in Table 4, those three substances have no effect on CYP450 2C9, CYP450 2D6, CYP450 3A4, CYP450 1A2, and CYP450 2C19, indicating that those three small molecules entering the body to participate in the metabolism will not cause the pharmacokinetics of CYP enzyme metabolism disorder. In addition, through the prediction of AMES Toxicity, Hepatotoxicity, and Carcinogenicity (Three-class), none of those three compounds were toxic. In summary, those three compounds all show good ADMET characteristics [56], which lays the foundation for further experiments.

3.4. Biolayer interferometry bingding (BLI) analysis

According to the results of previous studies [57,58] and the above molecular simulations, the RBD domain of SARS-CoV-2 binds with human ACE2 with high affinity. Therefore, the RBD domain becomes a

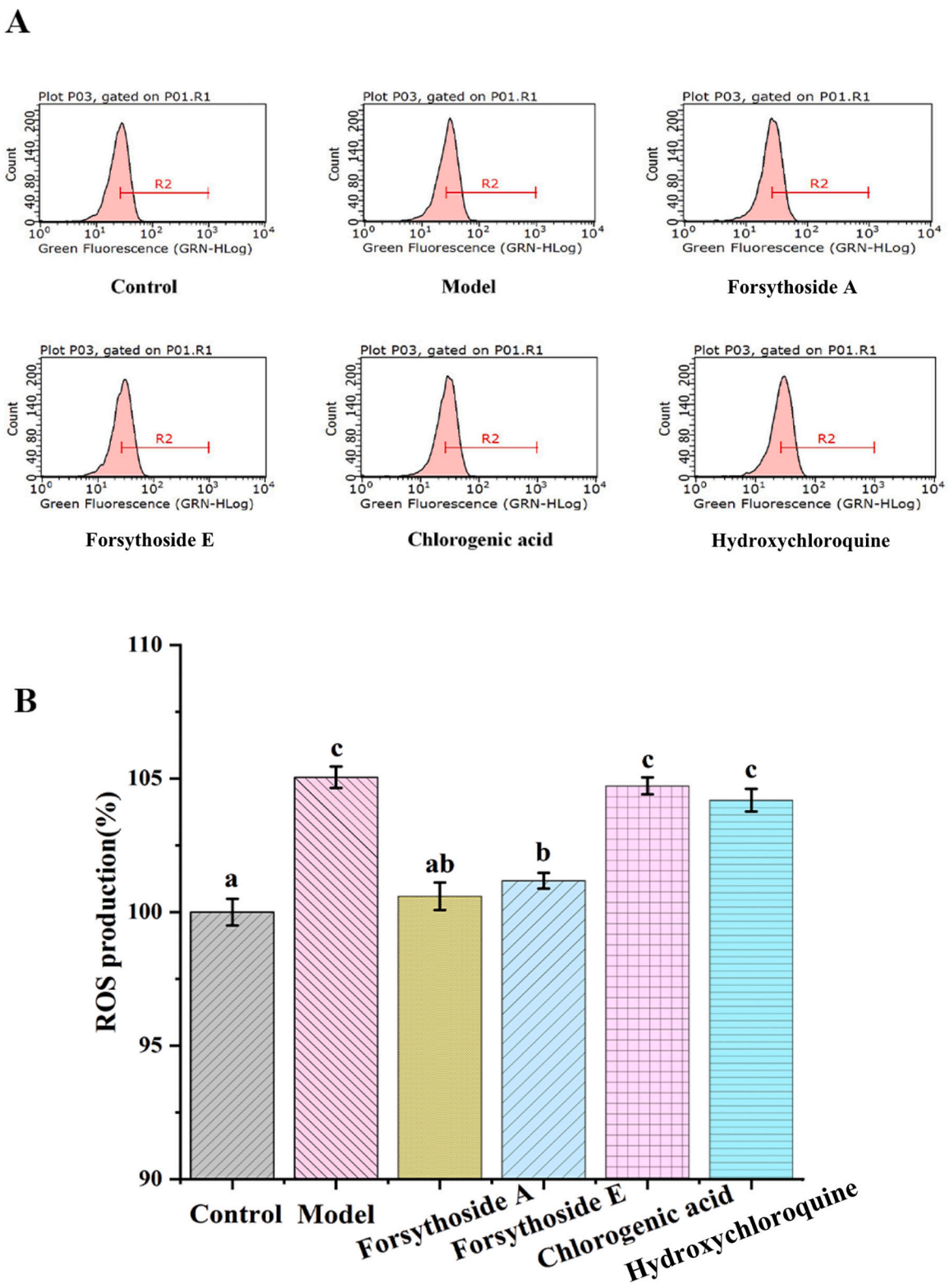

Fig. 7. Effects of forsythoside A, forsythoside E, chlorogenic acid, and hydroxychloroquine on AGEs induced EA.hy926 Cellular ROS inhibition of cells. Values are expressed as mean ± SD of triplicate replicates. Different letters indicate significant differences ($p < 0.05$).

potential target for blocking the binding of S protein to ACE2 in humans. In this study, Octet non-labeled interaction instrument was used to detect the binding affinity of SARS-CoV-2 spike protein (RBD, His Tag) with human ACE2 protein (Fc Tag) and compounds (forsythoside A/ forsythoside E/chlorogenic acid/hydroxychloroquine). As shown in Fig. 6A, 50 μg/mL of RBD combined with different concentrations of ACE2, showing high affinity ($K_D = 1 \times 10^{-12}$ (M) , $K_{on} = 1.89 \times 10^4$ (Ms^{-1}), $K_{off} = 1.89 \times 10^{-8}$ (s^{-1})). The high affinity of the binding again indicated that RBD is the key functional component responsible for SARS-CoV-2 binding to ACE2 within the S1 subunit, which is consistent with many previous studies [2,4,5]. As can be seen from Fig. 6B, the binding force between ACE2 at 200 nM and RBD is much higher than

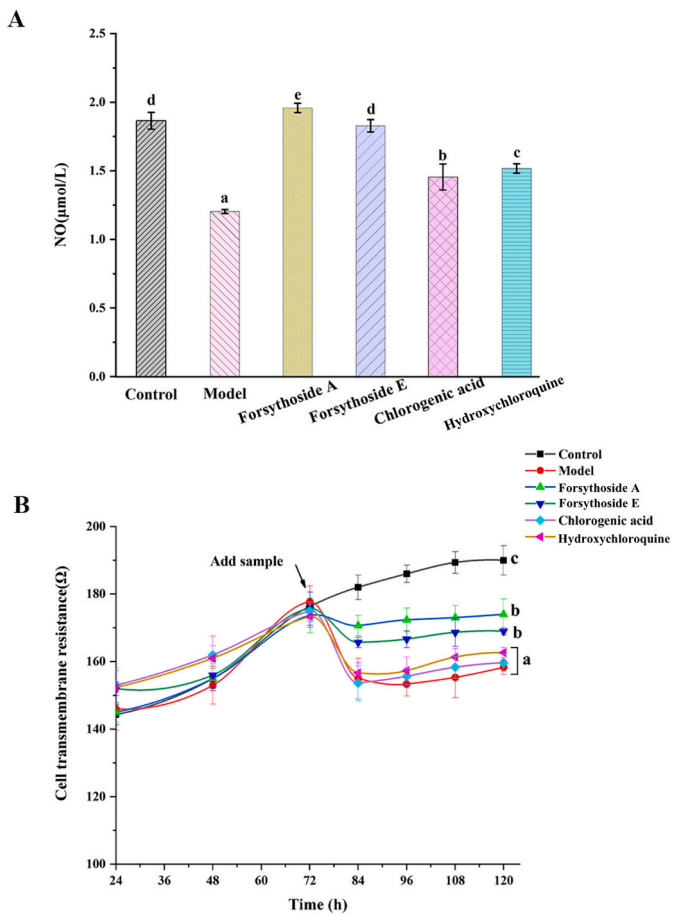

Fig. 8. AGEs-induced NO production and TEER value in EA.hy926 cells. A is the amounts of NO production by EA.hy926 cells by forsythoside A, forsythoside E, chlorogenic acid, and hydroxychloroquine. Values are expressed as mean ± SD of triplicate replicates. Different letters indicate significant differences ($p < 0.05$). B is the TEER (transepithelial electrical resistance) value of EA.hy926 cells cultured on the transwell plate was continuously monitored within 120 h. After 72 h of cell culture, the sample was added and the TEER value of cells was continuously monitored within 48 h after sample addition.

that of other compounds. For the four compounds (forsythoside A/forsythoside E/chlorogenic acid/hydroxychloroquine), only forsythoside A could combine with RBD, which indicated that forsythoside A may block or interfere with the binding of RBD to other receptors in the body (*e.g.*, ACE2) by binding to RBD, and this result was consistent with molecular docking studies that forsythoside A had a higher binding affinity with RBD). On this basis, the combination of different concentrations of forsythoside A with RBD was further determined. As can be seen from Fig. 6C, forsythoside A exhibited fast bonding and dissociation when interacted with RBD, and has a high affinity ($K_D = 4.79 \times 10^{-7}$ (M), $K_{on} = 2.29 \times 10^{3}$ (Ms^{-1}), $K_{off} = 1.09 \times 10^{-3}$ (s^{-1})). The high affinity of the substance is related to the concentration, and the binding effect can be achieved only when forsythoside A was at a certain concentration. In this study, RBD was only combined with forsythoside A at the concentration of 20 μM. Those results indicated that forsythoside A has potential anti-SARS-CoV-2 activity by effectively neutralizing the RBD domain of SARS-CoV-2 at a certain concentration. A previous study has shown that forsythoside A, as a key bioactive compound in traditional antiviral Chinese medicine, can fight influenza a virus by reducing the viral M1 protein [22]. Yu et al. also reported that natural compounds (*e.g.* glycyrrhizic acid) can disrupt the SARS-CoV-2-RBD/ACE2 interaction at low concentrations ($IC_{50} = 22$ μM), and can be used as a low-toxicity, broad-spectrum anti-coronavirus candidate [4].

3.5. AGEs-induced ROS, NO and TEER in EA.hy926 cells

It is found that diabetes is one of the diseases most associated with disease progression in patients with SARS-CoV-2 [12], which may be due to diabetic patients commonly accompany by more severe damage of vascular endothelial function. ACE2, as a binding target of virus invasion into the human body, is widely present in human vascular endothelial cells. When endothelial permeability and endothelial dysfunction increase, viruses are more likely to enter into the body by binding ACE2 in vascular endothelial cells and cause serious complications [14–16]. In this study, the protective effects of compounds (forsythoside A/forsythoside E/chlorogenic acid/hydroxychloroquine) against AGEs-induced endothelial dysfunction in EA.hy926 cells were comparatively studied by investigating ROS generation, NO production, and transepithelial electrical resistance (TEER) values.

Oxidative stress is defined as the excessive production of reactive oxygen species (ROS) in cells, including hydrogen peroxide, superoxide anion, *etc.* [46]. Excessive ROS induced by exogenous substances such as AGEs may disrupt the balance of cell redox, cause irreversible damage to the vascular endothelial cell, and thereby increase vascular endothelial permeability and dysfunction. As shown in Fig. 7, compared with the model group (treated with 800 μg/mL AGEs), forsythoside A and forsythoside E significantly inhibited ROS production ($p < 0.05$), especially forsythoside A, which had no significant difference in ROS production in comparison with the control group (800 μg/mL BSA) ($p > 0.05$). Those results indicated that forsythoside A, at 20 μM, could not only bind to the RBD domain but also inhibit oxidative stress in vascular endothelial cells (EA.hy926 cells) caused by AGEs. A previous study has also found that *F. suspensa* is an anti-inflammatory, antioxidant and antiviral plant [59], and its fruits and leaves can adjust the oxidative stress and pancreas insulin secretion caused by diabetes, thereby resisting diabetes [17].

Previous studies have shown that COVID-19 is a blood vessel disease; SARS-CoV-2 damages and attacks the vascular system at the cellular level, where blood vessels are thinner than elsewhere and even leak [60,61]. Therefore, it is particularly important to protect the vascular endothelial barrier. NO produced by eNOS has been shown to play an important role in protecting and maintaining vascular endothelial function. It is the most important regulator of vascular endothelial function, regulating endothelial function as a selective barrier between plasma and cell space [62]. As shown in Fig. 8A, NO production in the model group (treated with 800 μg/mL AGEs) was significantly decreased compared with that in the control group (treated with 800 μg/mL BSA) ($p < 0.05$). However, when compared with the model group, forsythoside A, forsythoside E, chlorogenic acid, and hydroxychloroquine all significantly increased the production of NO, especially forsythoside A, whose NO production was even higher than that of the control group ($p < 0.05$). The present results indicated that all those four substances may have the effect on protecting NO production in vascular endothelial cells to maintain vascular endothelial function, among which forsythoside A has the best effect. In addition, vascular barrier function can also be characterized by measuring the TEER value of endothelial cells on the transwell plate *in vitro* [46]. Therefore, the protective effects of four compounds on the barrier integrity of vascular endothelial cells were investigated by measuring the TEER value of EA.hy926 cells. As shown in Fig. 8C, the TEER value of the model group was significantly decreased compared with that of the control group ($p < 0.05$), indicating that the integrity of the monolayer of EA.hy926 cells was seriously damaged after induction of AGEs. Compared with the model group, forsythoside A and forsythoside E significantly increased the TEER value of the cell layer ($p < 0.05$), while the TEER values of chlorogenic acid and hydroxychloroquine had no significant improvement ($p > 0.05$). In conclusion, forsythoside A has a good role in maintaining vascular endothelial function and maintaining cytoskeleton stability, which is particularly important for protecting vascular endothelial function barriers and preventing blood leakage.

Table 5
Results of molecular docking of forsythoside A, forsythoside E, chlorogenic acid, hydroxychloroquine with profilin-1 receptor (PNF1, PDB: 3NUL).

Compounds for molecular docking	Affinity (kcal/mol)	Number of hydrophobic interactions	Amino acid residues involved in hydrophobic interactions	Number of hydrogen bonds	Amino acid residues involved in hydrogen bonds
Forsythoside A	−7.4 ± 0.0[d]	9	Asn18, Thr21, Ala22, Glu70, Lys87, Gly90, Phe105, Tyr106, Pro109	4	His19, Tyr72, Gly91, Glu108
Forsythoside E	−7.2 ± 0.1[c]	7	Thr21, Pro40, Gly68, Glu70, Pro89, Gly90, Phe105	4	Leu67, Tyr72, Gly91, Asp107
Chlorogenic acid	−5.8 ± 0.1[b]	5	Gly88, Tyr106, Glu108, Pro109, Thr111	3	Lys86, Pro89, Glu108
Hydroxychloroquine	−4.9 ± 0.1[a]	6	Gly30, Val32, Pro40, Gln41, Leu42, Ile47	1	Phe39

Affinity values are expressed as mean ± SD ($n = 3$). Different letters (a, b, c, d) indicated significant differences ($p < 0.05$).

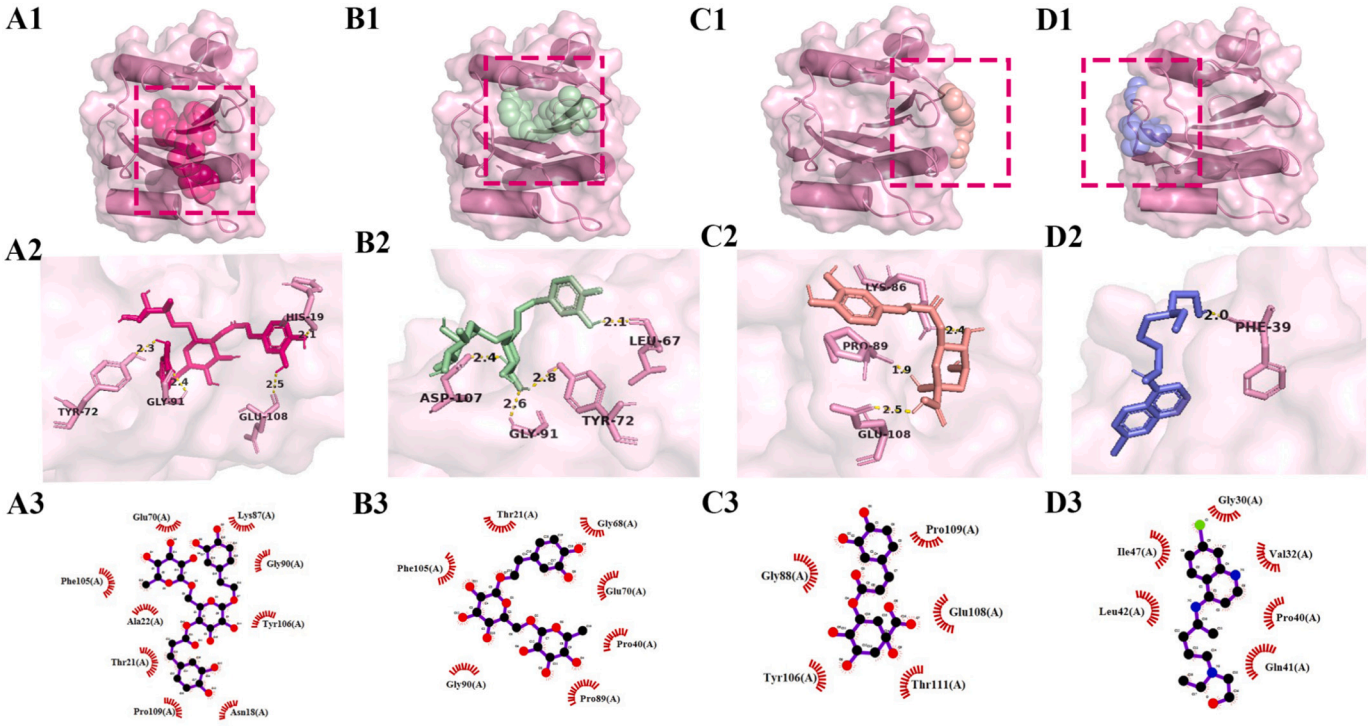

Fig. 9. The molecular docking diagram of the compound with the profilin-1 receptor (PNF1, PDB: 3NUL) is shown. In the figure, A\B\C\D respectively represent forsythoside A\forsythoside E\chlorogenic acid\hydroxychloroquine. The numbers 1\2\3 indicate the conformation\hydrogen bond\hydrophobic interaction of compounds and protein respectively.

3.6. Molecular docking studies for protective endothelial dysfunction

AGEs can induce recombination and redistribution of endothelial cytoskeleton actin, resulting in increased endothelial permeability [16]. PFN1 is thought to be the target molecule of AGEs-induced endothelial cell damage. Previous studies have shown that some small ligand molecules can regulate actin polymerization by binding PFN1 [33]. In this study, the interaction of forsythoside A, forsythoside E, chlorogenic acid, and hydroxychloroquine with PFN1 was studied through molecular docking analysis for clarifying the potential mechanism of their protection against AGEs induced endothelial cell injury. Table 5 and Fig. 9 show the docking parameters and the best docking conformation of the compound and PFN1 respectively. Fig. 9A showed the different locations of the four compounds in the PFN1 receptor, which are perfectly encapsulated in the receptor activity pocket. Results showed that the highest docking affinity energy with PFN1 among the four compounds was forsythoside A (− 7.4 ± 0.0 kcal/mol), followed by forsythoside E (− 7.2 ± 0.1 kcal/mol). The docking affinity of chlorogenic acid and hydroxychloroquine to PFN1 is very low, which is −5.8 ± 0.1 (kcal/mol) and -4.9 ± 0.1 (kcal/mol), respectively. This result indicated that forsythoside A was the most tightly binding to PFN1, and the affinity was significantly higher than the other three compounds ($p < 0.05$), while chlorogenic acid and hydroxychloroquine had almost no binding effect to the receptor. In addition, as shown in Fig. 9B and C, forsythoside A generated 9 hydrogen bonds and 4 hydrophobic interactions with amino acid residues of PFN1, and forsythoside E also generated 7 hydrogen bonds and 4 hydrophobic interactions with amino acid residues of PFN1. However, hydroxychloroquine only produced 6 hydrogen bonds and 1 hydrophobic interaction with PFN1 amino acid residues. Those results may to some extent explain the differences in the protective function of these compounds against AGEs-induced vascular endothelial dysfunction. A previous study has shown that hydrogen bond number and hydrophobic interaction are important indicators of ligand and receptor binding [63]. In addition, PFN1 mainly binds actin monomers to form the actin cytoskeleton. When the receptor scaffold binds to the ligand, this process affects its integrity and endocytosis [33]. This suggested that forsythoside A may protect against endothelial cell injury by binding to PFN1 to prevent or improve the recombination and redistribution of the endothelial cytoskeleton.

4. Conclusion

Based on *in vitro* and *in silicon* analyses, this study revealed that the bioactivities of several key proteins of COVID-19 and its variants, as well

as diabetic endothelial dysfunctions, were interfered by the main compounds, forsythoside A, in *F. suspensa* leaves. Results showed that the invasion and replication of SARS-CoV-2 and its variants could be inhibited by the compound forsythoside A through multiple protein targets. Molecular docking analysis showed that the proteins SARS-CoV-2-RBD-hACE2 of COVID-19 and its variants (Alpha (B.1.1.7), Beta (B.1.351) and Delta (B.1.617)), neuropilin-1 (NRP1), and SARS-CoV-2 main protease (M^{Pro}) were obviously interfered by the main ingredients in the leaves, especially forsythoside A. In the molecular dynamics study, each protein receptor of the virus could be stably bound by forsythoside A, especially in Delta (B.1.617) system, indicating the docking results were reliable. The RBD of COVID-19 was effectively combined by forsythoside A at 20 μM, and forsythoside A (20 μM) significantly inhibited intracellular ROS, increasing NO production and maintaining endothelial cell permeability in AGEs-induced EA.hy926 cells, and showed strong binding affinity to PFN1 protein associated with endothelial function. Results obtained in this study may provide some new knowledge and understanding for further understanding the role of interfering with the bioactivities of those key proteins of COVID-19/variants for diabetic patients to deal with the virus outbreak.

CRediT authorship contribution statement

Yishan Fu: Investigation, Data curation, Writing – original draft. **Fei Pan:** Investigation, Data curation, Writing – review & editing. **Lei Zhao:** Data curation. **Shuai Zhao:** Investigation. **Junjie Yi:** Methodology. **Shengbao Cai:** Conceptualization, Supervision.

Declaration of competing interest

The authors declare no conflicts of interest

Acknowledgements

The present work was financially supported by the National Natural Science Foundation of China (Grant Nos. 31960477 and 31901711) and the Natural Science Foundation of Yunnan Province (No. 2019FD051).

Appendix A. Supplementary data

Supplementary data to this article can be found online at https://doi.org/10.1016/j.ijbiomac.2022.03.145.

References

[1] A. Zhu, Z. Chen, Y. Wang, Q. Zeng, J. Sun, Z. Zhuang, N. Zhong, Immune responses to SARS-CoV-2 infection in humans and ACE2 humanized mice, Fundam. Res. (2021), https://doi.org/10.1016/j.fmre.2021.03.001.

[2] H.A. Odhar, S.W. Ahjel, A. Albeer, A.F. Hashim, A.M. Rayshan, S.S. Humadi, Molecular docking and dynamics simulation of FDA approved drugs with the main protease from 2019 novel coronavirus, Bioinformation 16 (2020) 236, https://doi.org/10.6026/97320630016236.

[3] E.M. Marinho, J.B. de Andrade Neto, J. Silva, C.R. da Silva, B.C. Cavalcanti, E. S. Marinho, H.V.N. Júnior, Virtual screening based on molecular docking of possible inhibitors of Covid-19 main protease, Microb. Pathog. 148 (2020), 104365, https://doi.org/10.1016/j.micpath.2020.104365.

[4] S. Yu, Y. Zhu, J. Xu, G. Yao, P. Zhang, M. Wang, J. Zhang, Glycyrrhizic acid exerts inhibitory activity against the spike protein of SARS-CoV-2, Phytomedicine 85 (2021), 153364, https://doi.org/10.1016/j.phymed.2020.153364.

[5] G. Simmons, P. Zmora, S. Gierer, A. Heurich, S. Pöhlmann, Proteolytic activation of the SARS-coronavirus spike protein: cutting enzymes at the cutting edge of antiviral research, Antivir. Res. 100 (2013) 605–614, https://doi.org/10.1016/j.antiviral.2013.09.028.

[6] S.N. Ladhani, G. Ireland, F. Baawuah, J. Beckmann, I.O. Okike, S. Ahmad, M. E. Ramsay, Emergence of SARS-CoV-2 Alpha (B.1.1.7) variant, infection rates, antibody seroconversion and seroprevalence rates in secondary school students and staff: active prospective surveillance, December 2020 to March 2021, MedRxiv, England, 2021. https://doi.org/10.1016/j.jinf.2021.08.019.

[7] S.A. Madhi, V. Baillie, C.L. Cutland, M. Voysey, A.L. Koen, L. Fairlie, A. Izu, Safety and efficacy of the ChAdOx1 nCoV-19 (AZD1222) Covid-19 vaccine against the B. 1.351 variant in South Africa, MedRxiv, 2021. https://doi.org/10.1101/2021.02.10.21251247.

[8] K. Yaniv, E. Ozer, A. Kushmaro, SARS-CoV-2 variants of concern, Gamma (P. 1) and Delta (B.1.617), sensitive detection and quantification in wastewater employing direct RT-qPCR, MedRxiv, 2021. https://doi.org/10.1101/2021.07.14.21260495v1.

[9] X. Tian, C. Li, A. Huang, S. Xia, S. Lu, Z. Shi, T. Ying, Potent binding of 2019 novel coronavirus spike protein by a SARS coronavirus-specific human monoclonal antibody, Emerg. Microbes Infect. 9 (2020) 382–385, https://doi.org/10.1080/22221751.2020.1729069.

[10] L. Cantuti-Castelvetri, R. Ojha, L.D. Pedro, M. Djannatian, J. Franz, S. Kuivanen, M. Simons, Neuropilin-1 facilitates SARS-CoV-2 cell entry and infectivity, Science 370 (2020) 856–860, https://doi.org/10.1126/science.abd2985.

[11] C.H. Mazucanti, J.M. Egan, SARS-CoV-2 disease severity and diabetes: why the connection and what is to be done, Immun. Ageing 17 (2020) 1–11, https://doi.org/10.1186/s12979-020-00192-y.

[12] R. Muniyappa, S. Gubbi, COVID-19 pandemic, coronaviruses, and diabetes mellitus, Am. J. Physiol. Endocrinol. Metab. 318 (2020), https://doi.org/10.1152/ajpendo.00124.2020. E736-E741.

[13] A. DeLoach, M. Cozart, A. Kiaei, M. Kiaei, A retrospective review of the progress in amyotrophic lateral sclerosis drug discovery over the last decade and a look at the latest strategies, Expert Opin. Drug Discovery 10 (2015) 1099–1118, https://doi.org/10.1517/17460441.2015.1067197.

[14] Z. Varga, A.J. Flammer, P. Steiger, M. Haberecker, R. Andermatt, A.S. Zinkernagel, H. Moch, Endothelial cell infection and endotheliitis in COVID-19, Lancet 395 (2020) 1417–1418, https://doi.org/10.1016/S0140-6736(20)30937-5.

[15] R. Horton, Offline: COVID-19—bewilderment and candour, Lancet (London, England) 395 (2020) 1178, https://doi.org/10.1016/S0140-6736(20)30850-3.

[16] F. Zhou, T. Yu, R. Du, G. Fan, Y. Liu, Z. Liu, B. Cao, Clinical course and risk factors for mortality of adult inpatients with COVID-19 in Wuhan, China: a retrospective cohort study, Lancet 395 (2020) 1054–1062, https://doi.org/10.1016/S0140-6736(20)30566-3.

[17] Y. Zhang, F. Feng, T. Chen, Z. Li, Q.W. Shen, Antidiabetic and antihyperlipidemic activities of Forsythia suspensa (Thunb.) vahl (fruit) in streptozotocin-induced diabetes mice, J. Ethnopharmacol. 192 (2016) 256–263, https://doi.org/10.1016/j.jep.2016.07.002.

[18] A. Mollica, G. Zengin, M. Locatelli, A. Stefanucci, A. Mocan, G. Macedonio, E. Novellino, Anti-diabetic and anti-hyperlipidemic properties of Capparis spinosa L.: in vivo and in vitro evaluation of its nutraceutical potential, J. Funct. Foods 35 (2017) 32–42, https://doi.org/10.1016/j.jff.2017.05.001.

[19] A. Mollica, G. Zengin, M. Locatelli, A. Stefanucci, A. Mocan, G. Macedonio, E. Novellino, An assessment of the nutraceutical potential of Juglans regia L. leaf powder in diabetic rats, Food Chem. Toxicol. 107 (2017) 554–564, https://doi.org/10.1016/j.fct.2017.03.056.

[20] K.L. Xiang, R.X. Liu, L. Zhao, Z.P. Xie, S.M. Zhang, S.J. Dai, Labdane diterpenoids from Forsythia suspensa with anti-inflammatory and anti-viral activities, Phytochemistry 173 (2020), 112298, https://doi.org/10.1016/j.phytochem.2020.112298.

[21] A.H.Y. Law, C.L.H. Yang, A.S.Y. Lau, G.C.F. Chan, Antiviral effect of forsythoside a from Forsythia suspensa (Thunb.) vahl fruit against influenza a virus through reduction of viral M1 protein, J. Ethnopharmacol. 209 (2017) 236–247, https://doi.org/10.1016/j.jep.2017.07.015.

[22] C. Ye, M. Gao, W. Lin, K. Yu, P. Li, G. Chen, Theoretical Study of the Anti-NCP Molecular Mechanism of Traditional Chinese Medicine Lianhua-Qingwen Formula (LQF), 2020, https://doi.org/10.26434/chemrxiv.12016236.

[23] Y. Ding, Z. Cao, L. Cao, G. Ding, Z. Wang, W. Xiao, Antiviral activity of chlorogenic acid against influenza a (H1N1/H3N2) virus and its inhibition of neuraminidase, Sci. Rep. 7 (2017) 1–11, https://doi.org/10.1038/srep45723.

[24] L. Runfeng, H. Yunlong, H. Jicheng, P. Weiqi, M. Qinhai, S. Yongxia, Y. Zifeng, Lianhuaqingwen exerts anti-viral and anti-inflammatory activity against novel coronavirus (SARS-CoV-2), Pharmacol. Res. 156 (2020), 104761, https://doi.org/10.1016/j.phrs.2020.104761.

[25] K. Hu, W.J. Guan, Y. Bi, W. Zhang, L.J. Li, N.S. Zhong, Efficacy and safety of lianhuaqingwen capsules, a repurposed chinese herb, in patients with coronavirus disease 2019: a multicenter, prospective, randomized controlled trial, Phytomedicine (2020), https://doi.org/10.1016/j.phymed.2020.153242.

[26] M.A. Larkin, G. Blackshields, N.P. Brown, R. Chenna, P.A. McGettigan, H. McWilliam, F. Valentin, I.M. Wallace, A. Wilm, R. Lopez, J.D. Thompson, T. J. Gibson, D.G. Higgins, Clustal W and clustal X version 2.0, Bioinformatics 23 (2007) 2947–2948, https://doi.org/10.1093/bioinformatics/btm404.

[27] B. Webb, A. Sali, Comparative protein structure modeling using MODELLER, Curr. Protoc. Bioinformatics 54 (2016) 5–6, https://doi.org/10.1002/0471250953.bi0506s15.

[28] M.U. Johansson, V. Zoete, O. Michielin, N. Guex, Defining and searching for structural motifs using DeepView/Swiss-PdbViewer, Bmc Bioinformatics 13 (2012) 173, https://doi.org/10.1186/1471-2105-13-173.

[29] O. Trott, A.J. Olson, AutoDock Vina: improving the speed and accuracy of docking with a new scoring function, efficient optimization, and multithreading, J. Comput. Chem. 31 (2010) 455–461, https://doi.org/10.1002/jcc.21334.

[30] A. Ali, R. Vijayan, Dynamics of the ACE2–SARS-CoV-2/SARS-CoV spike protein interface reveal unique mechanisms, Sci. Rep.-UK 10 (2020) 1–12, https://doi.org/10.1101/2020.06.10.143990.

[31] M. Calcagnile, P. Forgez, A. Iannelli, C. Bucci, M. Alifano, P. Alifano, ACE2 Polymorphisms and Individual Susceptibility to SARS-CoV-2 Infection: Insights From an in Silico Study, BioRxiv, 2020. https://doi.org/10.1101/2020.04.23.057042.

[32] S. Gul, In silico drug repositioning against human NRP1 to block SARS-CoV-2 host entry, J. Biol. Chem. (2020), https://doi.org/10.26434/chemrxiv.13425005.

[33] W. Witke, The role of profilin complexes in cell motility and other cellular processes, Trends Cell Biol. 14 (2004) 461–469, https://doi.org/10.1016/j.tcb.2004.07.003.
[34] A. Volkamer, D. Kuhn, T. Grombacher, F. Rippmann, M. Rarey, Combining global and local measures for structure-based druggability predictions, J. Chem. Inf. Model. 52 (2012) 360, https://doi.org/10.1021/ci200454v.
[35] R.A. Laskowski, M.B. Swindells, LigPlot+: multiple ligand-protein interaction diagrams for drug discovery, J. Chem. Inf. Model. 51 (2011) 2778–2786, https://doi.org/10.1021/ci200227u.
[36] D. Van Der Spoel, E. Lindahl, B. Hess, G. Groenhof, A.E. Mark, H.J. Berendsen, GROMACS: fast, flexible, and free, J. Comput. Chem. 26 (2005) 1701–1718, https://doi.org/10.1002/jcc.20291.
[37] F. Pan, L. Zhao, S. Cai, X. Tang, A. Mehmood, F. Alnadaria, & X. Ai, Prediction and evaluation of the 3D structure of Macadamia integrifolia antimicrobial protein 2 (MiAMP2) and its interaction with palmitoleic acid or oleic acid: An integrated computational approach, Food Chem. 367 (2021), 130677, https://doi.org/10.1016/j.foodchem.2021.130677.
[38] Y. Liu, G. Xu, J. Zhou, J. Ni, L. Zhang, X. Hou, Y. Ni, Structure-guided engineering of d-carbamoylase reveals a key loop at substrate entrance tunnel, ACS Catal. 10 (2020) 12393–12402, https://doi.org/10.1021/acscatal.0c02942.
[39] C. Lefebvre, G. Rubez, H. Khartabil, J.C. Boisson, J. Contreras-García, E. Hénon, Accurately extracting the signature of intermolecular interactions present in the NCI plot of the reduced density gradient versus electron density, Phys. Chem. Chem. Phys. 19 (2017) 17928–17936, https://doi.org/10.1039/c7cp02110k.
[40] H. Yang, C. Lou, L. Sun, J. Li, Y. Cai, Z. Wang, Y. Tang, admetSAR 2.0: web-service for prediction and optimization of chemical ADMET properties, Bioinformatics 35 (2019) 1067–1069, https://doi.org/10.1093/bioinformatics/bty707.
[41] D.E. Pires, T.L. Blundell, D.B. Ascher, pkCSM: predicting small-molecule pharmacokinetic and toxicity properties using graph-based signatures, J. Med. Chem. 58 (2015) 4066–4072, https://doi.org/10.1021/acs.jmedchem.5b00104.
[42] A. Daina, O. Michielin, V. Zoete, SwissADME: a free web tool to evaluate pharmacokinetics, drug-likeness and medicinal chemistry friendliness of small molecules, Sci. Rep.-UK 7 (2017) 1–13, https://doi.org/10.1038/srep42717.
[43] J.V. Dzimianski, N. Lorig-Roach, S.M. O'Rourke, D.L. Alexander, J.M. Kimmey, R. M. DuBois, Rapid and sensitive detection of SARS-CoV-2 antibodies by biolayer interferometry, Sci. Rep.-UK 10 (2020) 1–12, https://doi.org/10.1038/s41598-020-78895-x.
[44] L. Zeng, H. Ding, X. Hu, G. Zhang, D. Gong, Galangin inhibits α-glucosidase activity and formation of non-enzymatic glycation products, Food Chem. 271 (2019) 70–79, https://doi.org/10.1016/j.foodchem.2018.07.148.
[45] G. Gerardi, M. Cavia-Saiz, M.D. Rivero-Pérez, M.L. González-SanJosé, P. Muñiz, The protective effects of wine pomace products on the vascular endothelial barrier function, Food Funct. 11 (2020) 7878–7891, https://doi.org/10.1039/D0FO01199A.
[46] C.C. Wu, P.Y. Lai, S. Hsieh, C.C. Cheng, S.L. Hsieh, Suppression of carnosine on adhesion and extravasation of human colorectal cancer cells, Anticancer Res. 39 (2019) 6135–6144. https://doi.org/10.21873/anticanres.13821.
[47] R. Yan, Y. Zhang, Y. Guo, L. Xia, Q. Zhou, Structural basis for the recognition of the 2019-nCoV by human ACE2, BioRxiv, 2020. https://doi.org/10.1101/2020.02.19.956946.
[48] J.L. Daly, B. Simonetti, K. Klein, K.E. Chen, M.K. Williamson, C. Antón-Plágaro, Y. Yamauchi, Neuropilin-1 is a host factor for SARS-CoV-2 infection, Science 370 (2020) 861–865, https://doi.org/10.1126/science.abd3072.
[49] F. Pan, J. Li, L. Zhao, T. Tuersuntuoheti, A. Mehmood, N. Zhou, W. Lin, A molecular docking and molecular dynamics simulation study on the interaction between cyanidin-3-O-glucoside and major proteins in cow's milk, J. Food Biochem. 45 (2021), e13570, https://doi.org/10.1111/jfbc.13570.
[50] G. Pascarella, A. Strumia, C. Piliego, F. Bruno, R. Del Buono, F. Costa, F.E. Agrò, COVID-19 diagnosis and management: a comprehensive review, J. Intern. Med. 288 (2020) 192–206, https://doi.org/10.1111/joim.13091.
[51] J. Shang, G. Ye, K. Shi, Y. Wan, C. Luo, H. Aihara, F. Li, Structural basis of receptor recognition by SARS-CoV-2, Nature 581 (2020) 221–224, https://doi.org/10.1038/s41586-020-2179-y.
[52] F. Mehranfar, A.K. Bordbar, H. Parastar, A combined spectroscopic, molecular docking and molecular dynamic simulation study on the interaction of quercetin with β-casein nanoparticles, J. Photochem. Photobiol. B 127 (2013) 100–107, https://doi.org/10.1016/j.jphotobiol.2013.07.019.
[53] Y. Ghayeb, M. Sahihi, An investigation of molecular dynamics simulation and molecular docking: interaction of citrus flavonoids and bovine p-lactoglobulin in focus, Comput. Biol. Med. (2014), https://doi.org/10.1016/j.compbiomed.2014.04.022.
[54] S. Gholami, B. Abdol-Khalegh, Exploring binding properties of naringenin with bovine β-lactoglobulin: A fluorescence, molecular docking and molecular dynamics simulation study, Biophys. Chem. 187–188 (2014) 33–42, https://doi.org/10.1016/j.bpc.2014.01.003.
[55] G. Bocci, S. Verma, M.M. Hassan, J. Holmes, J.J. Yang, S. Sirimulla, T.I. Oprea, A machine learning platform to estimate anti-SARS-CoV-2 activities, Nat. Mach. Intell. (2021) 1–9, https://doi.org/10.1038/s42256-021-00335-w.
[56] U. Norinder, C. Bergström, A Prediction of ADMET properties, Chem. Med. Chem. 1 (2006) 920–937, https://doi.org/10.1002/chin.200646278.
[57] M. Vogel, G. Augusto, X. Chang, X. Liu, D. Speiser, M. Mohsen, M. Bachmann, Molecular definition of SARS-CoV-2 RBD mutations: receptor affinity versus neutralization of receptor interaction, Authorea Preprints, 2021. https://doi.org/10.22541/au.161903777.71370484/v1.
[58] C. Kim, D.K. Ryu, J. Lee, Y.I. Kim, J.M. Seo, Y.G. Kim, S.Y. Lee, A therapeutic neutralizing antibody targeting receptor binding domain of SARS-CoV-2 spike protein, Nat. Commun. 12 (2021) 1–10, https://doi.org/10.1038/s41467-020-20602-5.
[59] H. Qu, Y. Zhang, Y. Wang, B. Li, W. Sun, Antioxidant and antibacterial activity of two compounds (forsythiaside and forsythin) isolated from Forsythia suspensa, J. Pharm. Pharmacol. 60 (2008) 261–266, https://doi.org/10.1211/jpp.60.2.0016.
[60] H.K. Siddiqi, P. Libby, P.M. Ridker, COVID-19–a vascular disease, Trends Cardiovas. Med. (2020), https://doi.org/10.1016/j.tcm.2020.10.005.
[61] V. Lambadiari, F. Kousathana, A. Raptis, K. Katogiannis, A. Kokkinos, I. Ikonomidis, Pre-existing cytokine and NLRP3 inflammasome activation and increased vascular permeability in diabetes: a possible fatal link with worst COVID-19 infection outcomes, Front. Immunol. 11 (2020) 3063, https://doi.org/10.3389/fimmu.2020.557235.
[62] Y.P. Hwang, H.G. Kim, T.T. Hien, M.H. Jeong, T.C. Jeong, H.G. Jeong, Puerarin activates endothelial nitric oxide synthase through estrogen receptor-dependent PI3-kinase and calcium-dependent AMP-activated protein kinase, Toxicol. Appl. Pharm. 257 (2011) 48–58, https://doi.org/10.1016/j.taap.2011.08.017.
[63] S. Sriramoju, K. Goetz, Molecular docking interaction between carotenoids and curcumin and RAGE receptor prevents diabetic retinopathy progression (P06-044-19), Curr. Dev. Nutr. 3 (2019), https://doi.org/10.1093/cdn/nzz031.P06-044-19 nzz031-P06.